Determining Shape and Reflectance of Lambertian, Specular, and Hybrid Surfaces using Extended Sources

Shree K. Nayar, Katsushi Ikeuchi, and Takeo Kanade

The Robotics Institute, Carnegie Mellon University, Pittsburgh, PA 15213

Abstract

All existing shape extraction techniques that are based on photometric measurements rely on assumed surface reflection properties. We present a method for determining the shape of surfaces whose reflectance properties may vary from Lambertian to specular, without prior knowledge of the relative strengths of the Lambertian and specular components of reflection. The object surface is illuminated using extended light sources and is viewed from a single direction. Surface illumination using extended sources makes it possible to ensure the detection of both Lambertian and specular reflections. Multiple source directions are used to obtain an image sequence of the object. An extraction algorithm uses the set of image intensity values measured at each surface point to compute orientation as well as relative strengths of the Lambertian and specular reflection components. The proposed method has been named *photometric sampling* as it uses samples of a photometric function that relates image intensity to surface orientation, reflectance, and light source characteristics. Experiments were conducted on Lambertian surfaces, specular surfaces, and hybrid surfaces whose reflectance model is composed of both Lambertian and specular components. The results show high accuracy in measured orientations and estimated reflectance parameters.

1 Introduction

Shape from shading [4][6][9], photometric stereo [13][7][2], and local shape from specularity [3] are examples of techniques that extract three-dimensional shape information from photometric measurements. All of these techniques rely on prior knowledge of surface reflectance properties. In many vision applications, the reflectance properties of object surfaces are not readily available. Further, most existing methods are only capable of determining the shape of either Lambertian or specular surfaces. Many surfaces encountered in practice, are hybrid in reflectance; their reflectance model is a linear combination of Lambertian and specular models. Therefore, Lambertian and specular models are only limiting instances of the hybrid model. It is desirable to have a method that is capable of extracting the shape of Lambertian, specular, as well as hybrid surfaces.

Yet another limitation of all existing extraction methods is their inability to furnish information regarding the reflectance properties of the object surface. In many industrial applications, surface polish and surface roughness are found to be important inspection criteria. In such cases, surface reflectance properties may be interpreted as measures of surface polish and roughness. Further, reflectance properties may be used to segment an image in different regions; each region may be regarded as a different surface to aid the process of inspection. For these reasons, it would be of great value to have a technique that could, in addition to determining shape, also estimate the reflectance properties of each surface point.

This paper presents a method for determining the shape of objects whose surfaces may be Lambertian, specular, or hybrid. Shape information is extracted without prior knowledge of the relative strengths of the Lambertian and specular reflection components. The method also determines parameters that represent the reflectance properties of each surface point.

2 Photometric Sampling

2.1 Basic Photometric Function

Consider the illumination of an object by a point source of light, as shown in Figure 1. The point source emits light in all directions. Light energy reflected by the surface in the direction of the camera causes an image of the surface to be formed. For a given orientation of the surface and direction of the point source, the amount of light energy reflected by the surface in a particular direction is determined by its reflectance properties. The reflectance model of a large number of surfaces comprises two components, namely, the Lambertian (diffuse) component and the specular (gloss) component. Therefore, the intensity at any point in the image of the surface may be expressed as:

$$I = IL + IS, \qquad (1)$$

where IL is the Lambertian intensity component and IS is the specular intensity component.

We will express the two components of image intensity in terms of the parameters that describe the two-dimensional imaging and illumination geometry shown in Figure 1. In two dimensions, the source direction vector s, surface normal vector n, and viewing direction vector v lie in the same plane. Therefore, directions are represented by a single parameter, namely, the zenith angle θ.

Lambertian Reflection: The Lambertian intensity IL represents the *diffuse* component of reflection. Surfaces that satisfy Lambert's law appear equally bright from all directions. Broadly speaking, there are two mechanisms that produce Lambertian reflection. In one case,
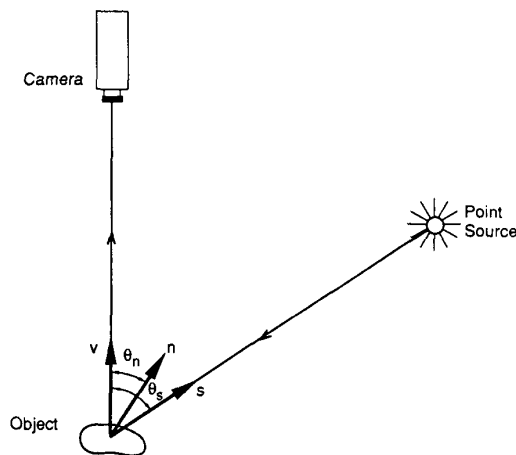

Figure 1: Two-dimensional illumination and imaging geometry. A surface element with orientation θ_n reflects light from the point source direction θ_s into the camera.

light rays that impinge the surface are reflected many times between surface undulations before they are scattered into space. If these *multiple reflections* occur in a random manner, the incident energy is distributed in all directions resulting in diffuse reflection. Another mechanism leading to diffuse reflection is the *internal scattering* of light rays. In this case, the light rays penetrate the surface and encounter microscopic inhomogeneities in the surface medium. The light rays are repeatedly reflected and refracted at boundaries between regions of differing refractive indices. Some of the scattered rays find their way back to the surface with a variety of directions resulting in diffuse reflection. When diffuse reflection produced by either or both of the above mechanisms results in constant surface radiance in all directions, we have Lambertian reflection. The brightness of a Lambertian surface is independent of the viewing direction. However, the brightness of a Lambertian surface is proportional to the energy of incident light. As seen in Figure 1, the amount of light energy falling on the surface element is proportional to the area of the surface element as seen from the source position, often referred to as the foreshortened area. The foreshortened area is a cosine function of the angle between the surface orientation direction θ_n and the source direction θ_s. Therefore the Lambertian intensity component IL may be written as:

$$IL = A\cos(\theta_s - \theta_n),\qquad(2)$$

where the constant A determines the fraction of incident energy that is diffusely reflected. We have assumed that the angle of incidence $(\theta_s - \theta_n)$ is greater than $-\pi/2$ and less than $\pi/2$, i.e. IL is always greater than zero.

Specular Reflection: Various specular reflectance models have been proposed over the years. We will use the Beckmann and Spizzichino model [1] that is based physical optics theory. The surface height is modeled as a continuous stationary random process with mean value zero and standard deviation σ_h that represents the physical *roughness* of the surface. Maxwell's equations are used to determine how incident light waves are scattered by the surface in various directions. Beckmann and Spizzichino have found specular reflection to be composed of two primary components: the *specular lobe component* and the *specular spike component*. The lobe component spreads around the specular direction $(\theta_s = 2\theta_s)$, and the spike component is zero in all directions except a very narrow range around the specular direction. The strengths of the two components are dependent on the ratio σ_h/λ, where λ is the wavelength of incident light. When $\sigma_h/\lambda \approx 0$, the spike component is many orders in magnitude greater than the lobe component and the surface reflects light like a mirror. It is the spike component that is responsible for strong highlights that are often observed on smooth surfaces. As σ_h/λ increases above unity, the spike component shrinks and the lobe component begins to dominate the surface radiance value. In this paper, we will assume that the surface is smooth $(\sigma_h/\lambda < 1.0)$, and the specular image intensity IS is solely determined by the spike component. Beckmann and Spizzichino have found that the spike component is mathematically represented by the square of a very sharp sinc function that tends to be symmetric with respect to the specular angle $\theta_s = 2\theta_n$. For simplicity, we shall approximate the spike component by the delta function:

$$IS = B\,\delta(\theta_s - 2\theta_n).\qquad(3)$$

The *basic photometric function*[1] relates image intensity to surface orientation, surface reflectance, and point source direction and may be written by substituting equations 2 and 3 in equation 1 as:

$$I = A\cos(\theta_s - \theta_n) + B\,\delta(\theta_s - 2\theta_n).\qquad(4)$$

The constants A and B in equation 4 represent the relative strengths of the Lambertian and specular components of reflection. We call A and B the reflection parameters. We see that, $A > 0$ and $B = 0$ for a purely Lambertian surface, $A = 0$ and $B > 0$ for a purely specular surface, and $A > 0$ and $B > 0$ for a hybrid surface.

Our objective is to determine orientation and reflectance at each surface point from a set of image intensities that result from changing the source direction θ_s. As seen in Figure 1, by moving the source around the object, we can vary the source direction without changing the orientation and reflectance parameters. Therefore,

even though the orientation and reflectance parameters are unknown, we can treat them as constants in equation 4. For this reason, we will often refer to the basic photometric function as $I(\theta_s)$, a relation between image intensity and source direction. Figure 2 shows a plot of the basic photometric function for a hybrid surface of given orientation.
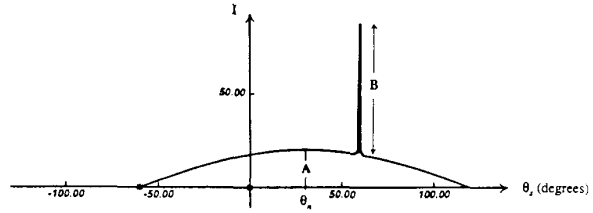

Figure 2: Basic photometric function $I(\theta_s)$ for a hybrid surface.

2.2 Why Extended Sources ?

We propose to illuminate the object surface by using extended sources, rather than point sources, for the following reasons:

- In the case of point source illumination, specular reflection is not detected unless $\theta_s = 2\theta_n$. In order to determine shape and reflectance parameters of specular and hybrid surfaces, specular reflections must be captured in the measured intensities. To detect specular reflections from surface points of all orientations, an infinite number of point sources need to be positioned around the surface. Such an approach is unrealistic from the perspective of practical implementation. Unlike a point source, an extended source emits light from an area of points rather than a single point. Therefore, a small number of extended sources may be used to ensure the detection of specular reflections.

- In the case of point source illumination, image intensities due to specular reflections are often observed to be much greater than intensities resulting from Lambertian reflections [10]. Therefore, it is difficult to measure both components in the same image. Extended source illumination tends to make the image intensities due to Lambertian and specular reflections comparable to one another. A specular surface element of a given orientation will reflect light from a small area on the extended source into the camera. On the other hand, a Lambertian surface element of the same orientation reflects light from all points on the extended source. This feature of the proposed illumination scheme makes it possible to measure both Lambertian and specular reflections in the same image.

2.3 Generating Extended Sources

There are numerous ways of generating extended sources. In this section, we present the approach that we have chosen to use. An extended light source can be generated by illuminating a sheet of light-diffusing material with a point light source. Figure 3 illustrates the illumination of a section of a circular diffuser of radius R. The point source is placed at a distance H from the diffuser's surface, and the viewed object is placed at the center of the circle. Let us assume that the diffuser is "ideal", i.e. incident energy is scattered equally in all directions. Therefore, the radiance[2] $L(\theta, \theta_s)$ of the inner surface of the diffuser is proportional to the irradiance[3] $E(\theta, \theta_s)$ of the outer surface of the diffuser:

$$L(\theta, \theta_s) = CE(\theta, \theta_s).\qquad(5)$$

---

[1]The photometric function is similar to the image irradiance [5] equation, since image intensity is assumed to be proportional to image irradiance.

[2]Radiance is defined as the flux emitted per unit foreshortened surface area per unit solid angle. Radiance is measured in watts per square meter per steradian $(W.m^{-2}.sr^{-1})$.

[3]Irradiance is defined as the incident flux density and is measured in watts per square meter $(W.m^{-2})$.

[4]Radiant Intensity of a source is defined as the flux exiting per unit solid angle and is measured in watts per steradian $(W.sr^{-1})$.
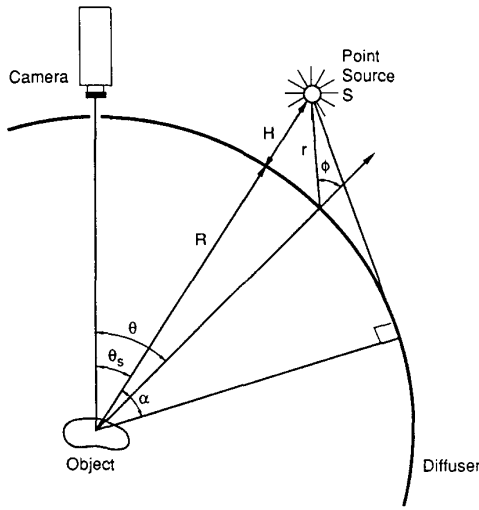
Figure 3: An extended source.

where C is a constant of proportionality. The analytic expression for the surface irradiance $E(\theta, \theta_s)$ may be derived from the basics of radiometry as:

$$E(\theta, \theta_s) = \frac{I\cos\phi}{r^2} \qquad (6)$$

where I is the radiant intensity[4] of the point source S. The radiance of the extended source may be determined by expressing the variables r and ϕ in equation 6 in terms of the parameters R, H, and θ_s of the illumination geometry:

$$L(\theta, \theta_s) = \frac{CI[(R + H)\cos(\theta - \theta_s) - R]}{[(R + H - R\cos(\theta - \theta_s))^2 + (R\sin(\theta - \theta_s))^2]^{3/2}} \qquad (7)$$

Throughout this paper, the position of an extended source will be denoted by the angle θ_s of the point source used to generate the extended source. The radiance function $L(\theta, \theta_s)$ is symmetric, or even, with respect to the source direction $(\theta = \theta_s)$, and its magnitude decreases as θ deviates from θ_s. Points on the diffuser that lie in the interval $\theta_s - \alpha < \theta < \theta_s + \alpha$ receive light from the point source S. Points that lie outside this interval are occluded from the point source by points that lie in the interval. Thus, $L(\theta, \theta_s) = 0$ for $\theta < \theta_s - \alpha$ and $\theta > \theta_s + \alpha$. The *source termination angle* α is found from Figure 3 as:

$$\alpha = \cos^{-1}\frac{R}{R + H} . \qquad (8)$$

2.4 Photometric Function for Extended Sources

The photometric function for point source illumination (equation 4) needs to be modified for extended source illumination. An extended source may be thought of as a collection of point sources where each point source has a radiant intensity that is dependent on its position on the extended source. The intensity of light reflected by a surface may be determined by computing the integral of the light energies reflected from all points on the extended source. Therefore, the modified photometric function $I'(\theta_s)$ is determined by convolving the basic photometric function $I(\theta)$ with the extended source radiance function $L(\theta, \theta_s)$. This operation is illustrated in Figure 4. For a surface point of orientation θ_n, the Lambertian component IL' of the modified photometric function is determined as:

$$IL' = A \int_{\theta_s - \alpha}^{\theta_s + \alpha} L(\theta, \theta_s) \cos(\theta - \theta_n) \, d\theta . \qquad (9)$$

The limits of the integral are determined by the width of the extended source. It can be proved [8] that IL' is a cosine function of the angle between the surface orientation and the direction corresponding to
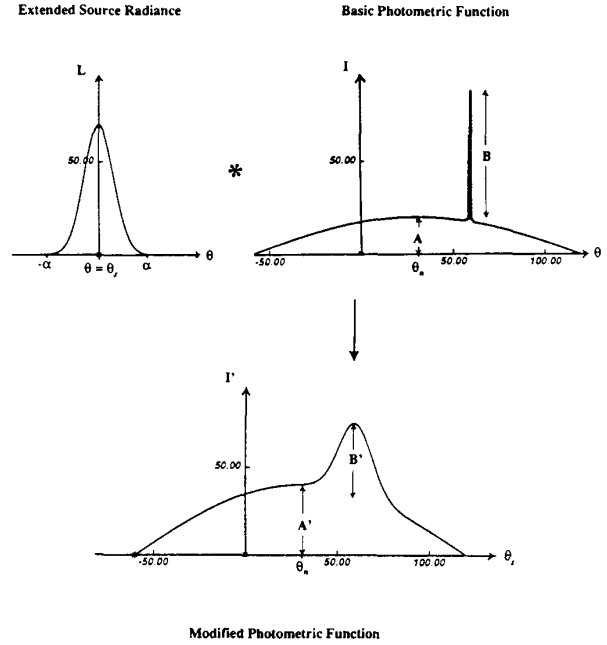
Figure 4: The photometric function for extended source illumination is obtained by convolving the basic photometric function with the extended source radiance function.

the "center of mass" of the extended source radiance distribution, $L(\theta, \theta_s)$. In our case, since the extended source is symmetric with respect to the direction θ_s, the center of mass of the radiance function is in the direction θ_s. Therefore, we obtain:

$$IL' = A' \cos(\theta_s - \theta_n) , \qquad (10)$$

where the constant A' represents the strength of the Lambertian component.

On similar lines, the specular intensity component IS' resulting from the extended source $L(\theta, \theta_s)$ is determined as:

$$IS' = B \int_{\theta_s - \alpha}^{\theta_s + \alpha} L(\theta, \theta_s)\, \delta(\theta - 2\theta_n)\, d\theta , \qquad (11)$$

or:

$$IS' = B\, L(2\theta_n, \theta_s) . \qquad (12)$$

Strictly speaking, the result of the above integral is dependent on the exact shape of the specular spike. However, since the spike component is significant only in the specular direction, $2\theta_n$, it is reasonable to assume that the specular intensity IS' is proportional to $L(2\theta_n, \theta_s)$, while the constant of proportionality is dependent on the exact shape of the spike. To this end, we will use the constant B', rather than B, to represent the strength of the specular component of the photometric function.

The *modified photometric function* relates image intensity I' to extended source direction θ_s, and is expressed as the sum of the components IL' and IS':

$$I' = A' \cos(\theta_s - \theta_n) + B' L(2\theta_n, \theta_s) . \qquad (13)$$

2.5 Sampling

The process of measuring image intensities corresponding to different source directions is equivalent to sampling the modified photometric function $I'(\theta_s)$, as shown in Figure 5. Samples of the photometric function may be obtained by moving an extended source around the object and taking images of the object for different source positions. An alternative approach would be to distribute an array of extended sources around the object such that each source illuminates

the object from a different direction. The entire array of extended sources may be sequentially scanned such that, for each scan, a single source is active and an image of the object surface is obtained. We will confine the sampling process to two dimensions; the surface normal vector, viewing direction vector, and source direction vectors for all extended sources, are coplanar. The sequential scanning of extended sources positioned in the directions $\{\theta_i: i=1,2,......M\}$ results in a set of image intensities $\{I'_i: i=1,2,......M\}$ measured at each point on the object surface.
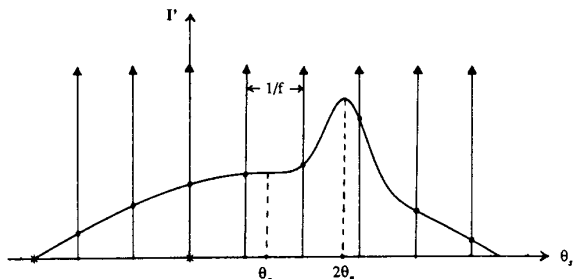
Figure 5: Sampling the modified photometric function.

The number of samples measured at each surface point is determined by the frequency f at which $I'(\theta_s)$ is sampled. In order to extract the shape and reflectance parameters of hybrid surfaces, both Lambertian and specular components of image intensity must be detected. Since we have used a delta function for specular reflection model, the period of the modified photometric function that contains specular intensities is equal to the width, 2α, of the extended source radiance function. In the following section, we will show that, in general, at least two photometric samples must have non-zero specular intensities for the extraction technique to work. Hence, the photometric function must be sampled at a frequency greater than or equal to the *minimum sampling frequency*[5] f_{min}, where:

$$f_{min} = \frac{1}{\alpha}.$$ (14)

Note that, at this minimum frequency, the radiance distributions of adjacent extended sources overlap each other for an interval of α.

3 Extracting Shape and Reflectance

Given the set of image intensities $\{I'_i\}$ measured at a surface point, we want to determine the orientation θ_n and reflectance parameters A' and B' of the point. We will first develop techniques to compute orientations of purely Lambertian and purely specular surfaces. Later, these techniques will be used as tools to extract orientations and reflectance parameters of hybrid surfaces.

3.1 Lambertian Surfaces

Consider the case where the surface of an object is known to be purely Lambertian, and the shape of the object is to be determined. The photometric samples for a Lambertian surface point may be written as:

$$I'_i = A' cos(\theta_i - \theta_n).$$ (15)

We would like to compute the orientation θ_n and the strength A' of Lambertian reflection component. To this end, an error E is formulated as the sum of the errors in measured samples over the entire set of samples:

$$E = \sum_{i=1}^{M} [I'_i - A' cos(\theta_i - \theta_n)]^2.$$ (16)

[5]It is assumed that the interval of the modified photometric function that contains specular intensities is small compared to the total width of the photometric function. Therefore, sampling frequencies that ensure the detection of specular intensities will provide a sufficient number of Lambertian intensity samples.

By using the conditions:

$$\frac{\partial E}{\partial \theta_n} = 0 \quad and \quad \frac{\partial E}{\partial A'} = 0,$$ (17)

we can determine values of θ_n and A' that minimize the error E.

3.2 Specular Surfaces

Now consider the case where the object surface is known to be purely specular, and the shape of the object is to be determined. The photometric samples for a specular point may be written as:

$$I'_i = B' L(2\theta_n, \theta_i).$$ (18)

We want to determine the orientation θ_n and the specular strength B' from the intensity set $\{I'_i\}$. Let us assume that the specular direction $2\theta_n$ lies between the directions θ_k and θ_{k+1} of two adjacent extended sources. Further, let us assume that the photometric function is sampled using the minimum frequency f_{min}, i.e. $\theta_{k+1} = \theta_k + \alpha$. Therefore, since the surface is specular only the samples I'_k and I'_{k+1} will have non-zero values. We see that when θ_n increases, $2\theta_n$ approaches θ_{k+1}, I'_k decreases, and I'_{k+1} increases. Similarly, when θ_n decreases, $2\theta_n$ approaches θ_k, I'_k increases, and I'_{k+1} decreases. In fact, from equation 18 we see that the intensity ratio I'_k/I'_{k+1} is equal to the ratio $L(2\theta_n, \theta_k)/L(2\theta_n, \theta_{k+1})$. Since the extended sources have decaying radiance functions (section 2.3), this ratio is a monotonic function of the angle $2\theta_n$. Since the radiance functions of the extended sources are known a-priori, we can precompute and store in memory the correspondence between I'_k/I'_{k+1} and θ_n.

Given the image intensity set $\{I'_i\}$ at a specular surface point, the non-zero image intensities in the set are first determined. If only a single intensity value, for instance I'_k, is greater than zero, then we know that $2\theta_n = \theta_k$. If two image intensities, for instance I'_k and I'_{k+1}, are greater than zero, the ratio I'_k/I'_{k+1} is used to determine θ_n. Once θ_n is found, B' is obtained by using equation 18:

$$B' = \frac{I'_k}{L(2\theta_n, \theta_k)}.$$ (19)

3.3 Hybrid Surfaces

The modified photometric function for hybrid surfaces is given by equation 13. At each surface point, we want to determine A', B', and orientation θ_n from the measured samples $\{I'_i: i=1,2,......M\}$ of the photometric function. To this end, we will develop an algorithm that attempts to separate the Lambertian and specular components af each measured image intensity, and computes surface orientations by using the methods given above for Lambertian and specular surfaces.

The extraction algorithm is based on two constraints, namely, the *sampling frequency constraint* and the *unique orientation constraint*. By sampling the modified photometric function at the minimum sampling frequency f_{min}, we can ensure that only two consecutive image intensities in the intensity set $\{I'_i\}$ contain non-zero specular components. For each k in the interval $0 < k < M$, I'_k and I'_{k+1} are hypothesized as being the two intensities that are corrupted by specular components. All remaining intensities in the set $\{I'_i: i=1,2,......M\}$ must represent only Lambertian components of reflection. These intensities are used to compute the surface orientation θ_{nl} and the Lambertian strength A' (section 3.1). The Lambertian components IL'_k and IL'_{k+1} are determined and used to separate the specular components IS'_k and IS'_{k+1} from I'_k and I'_{k+1}, respectively. The surface orientation θ_{ns} and specular strength B' are computed from IS'_k and IS'_{k+1} (section 3.2).

Next, the physical constraint that each surface point has a unique orientation is exploited. An estimate θ_{nk} of the orientation is found as a weighted average of the orientations θ_{nl} and θ_{ns}. The weights are proportionate to the strengths of the two components of reflection. We support this method of weight selection because the surface orientation that is computed from intensities resulting from the stronger of the two reflection components is less sensitive to image noises and is, therefore, more reliable. An orientation error e_k is found by comparing θ_{nk} with θ_{nl} and θ_{ns}. Using the above approach, orientation errors are computed for all k, where $0 < k$ $< M$. The orientation and reflectance parameters computed for the

value of k that minimizes the orientation error are assigned to the surface point under consideration. This process is repeated for all points on the object surface.

It is important to note that the extraction algorithm is not only capable of determining shape and reflectance properties of hybrid surface, but also purely Lambertian and purely specular surfaces.

Extraction Algorithm

Step 1: Let k = 1 and e_0 equal a large positive number.

Step 2: Hypothesize that image intensities I'_k and I'_{k+1} consist of specular components of reflection. All intensities I'_i, where $i \neq k$ and $i \neq k+1$, and the Lambertian model are used to compute the surface orientation θ_{al} and Lambertian strength A'_k (section 3.1).

Step 3: The specular components IS'_k and IS'_{k+1} are separated from the image intensities I'_k and I'_{k+1}.

$$IS'_k = I'_k - A'_k \cos(\theta_k - \theta_{al}),$$
$$IS'_{k+1} = I'_{k+1} - A'_k \cos(\theta_{k+1} - \theta_{al}). \quad (20)$$

If $IS'_k < 0$ or $IS'_{k+1} < 0$, set $k = k + 1$ and go to step 2.

Step 4: The surface orientation θ_{m} and the specular strength B'_k are determined by using specular intensities IS'_k and IS'_{k+1} and the specular model (section 3.2).

Step 5: The best estimate of surface orientation, for the kth iteration, is determined as:

$$\theta_{ok} = \frac{A'_k \theta_{al} + B'_k \theta_{m}}{A'_k + B'_k}. \quad (21)$$

The orientation error e_k is determined as:

$$e_k = \frac{A'_k |\theta_{al} - \theta_{ok}| + B'_k |\theta_{m} - \theta_{ok}|}{A'_k + B'_k}. \quad (22)$$

Step 6: If $e_k < e_{k-1}$, then:

$$\theta_o = \theta_{ok}, \quad A' = A'_k, \quad B' = B'_k. \quad (23)$$

If $k < M-1$, set $k = k + 1$ and go to step 2. Else, stop.

4 Experiments

We have conducted experiments to demonstrate the practical feasibility of the photometric sampling concept. A photograph of the experimental set-up used to implement photometric sampling, is shown in Figure 6. A 14-inch diameter lamp shade is used as the spherical diffuser, and extended light sources are generated on the diffuser's surface by illuminating it using incandescent light bulbs. All light bulbs are assumed to have the same radiant intensity and are equidistant from the center of the diffuser. A source termination angle of $\alpha = 32$ degrees is used, and sampling is performed at the minimum frequency determined by equation 14. The object is placed at the center of the diffuser and is viewed by a camera through a 1-inch diameter hole at the top of the diffuser. The current set-up uses a WV-22 model Panasonic CCD camera that has a 512×480 pixel resolution. The complete imaging system, comprising of lenses and camera, has a physical resolution of 0.002 inches per pixel width. In the current implementation, the light bulbs, camera, and object are all placed in the same plane. This two-dimensional set-up is only capable of measuring the orientation of surface normal vectors that lie on a single plane in orientation space. For each extended source, an image of the object is digitized and stored in memory. The sequence of object images, generated by scanning the array of extended sources, is processed on a 3/60 SUN work-station.

The experimental set-up and the extraction algorithm were used to extract surface properties of a number of objects. Figure 7, Figure 8, and Figure 9, show the results of the extraction method applied to objects with different surface reflectance properties. For each object, a photograph of the object is followed by two reflectance images and
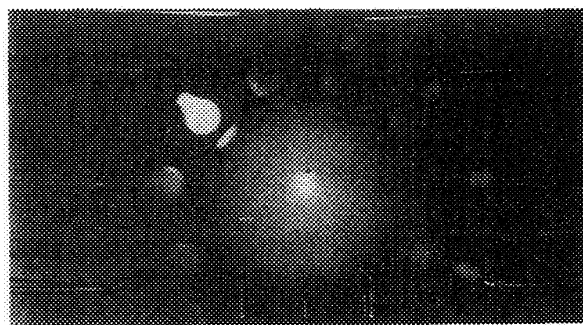

Figure 6: Photograph of the experimental set-up used to demonstrate the photometric sampling concept.

a needle map produced by the extraction algorithm, and a depth map that is reconstructed from the needle map. The reflectance properties of the surfaces are given by two images, namely, the Lambertian strength image and the specular strength image. The intensity at each pixel, in either of these two images, is proportional to the strength of the reflectance model component the image represents. The needle map is a representation of surface orientations. At each point on a needle map, the length of the needle is proportional to the tilt of the surface away from the viewing direction of the camera. The direction in which each needle points is determined by locating the starting point of the needle. All needles originate from the dots that constitute the resolution grid of the needle map. To help evaluate the performance of the extraction algorithm, we have included a depth map of each object that is obtained by integrating the orientations in the needle map. Note that the reconstructed surfaces are displayed at some off-set level in all the depth maps.

The object shown in Figure 7 is cylindrical and its surface is Lambertian. Figure 8 shows a prism-shaped object that has a highly specular surface. A major advantage of the photometric sampling method, over all existing shape extraction techniques, lies in its ability to determine the shape and reflectance of hybrid surfaces. The surfaces of many manufactured plastic objects seem to fall very well into this category. The Lambertian component is produced by the internal scattering mechanism, while the specular spike results from the smoothness of the surface. Figure 9 shows the photo of a cylindrical plastic object. As expected, non-zero Lambertian and specular strengths are seen in the reflection images. The needle and depth maps of the object are consistent with the actual shape.
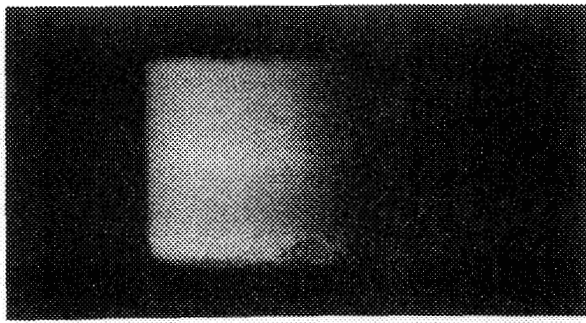
An important feature of all the above results is that the surface properties at a pixel are computed solely from the intensities recorded at that pixel. The needle maps and reflectance images have not been subjected to any filtering operations. A simple error analysis was conducted to estimate the measurement accuracy of the current set-up. In the results obtained so far, measured surface orientations were found to be within 4 degrees of the actual orientation values, and an average error of 2 degrees in orientation was estimated.
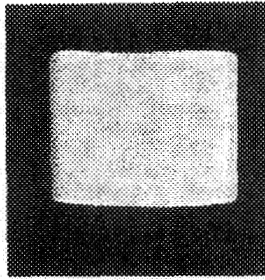
5 Conclusions

We conclude this paper with the following remarks:

- The photometric sampling method is capable of determining the shape and reflectance parameters of Lambertian, specular, and hybrid surfaces.

- The method is local in that orientation and reflectance of a surface point are computed solely from image intensities recorded at that point.

- Active surface illumination, using extended light sources, makes it possible to capture both Lambertian and specular reflections in the image intensities.

- Accurate orientation estimates are obtained by using both Lambertian and specular components of the image intensities.
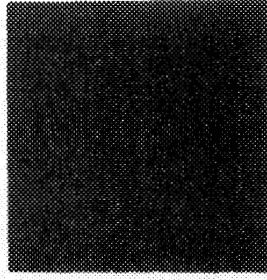
We are currently in the process of extending the theory and experimental set-up to three dimensions.
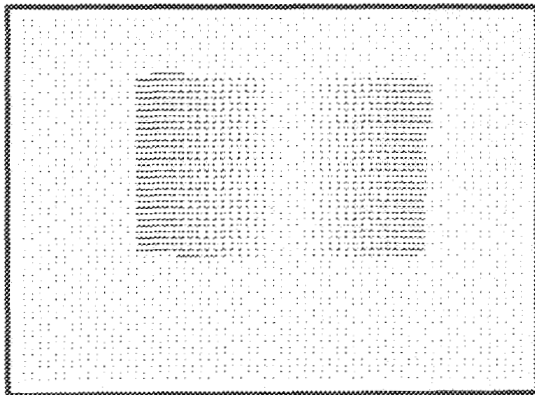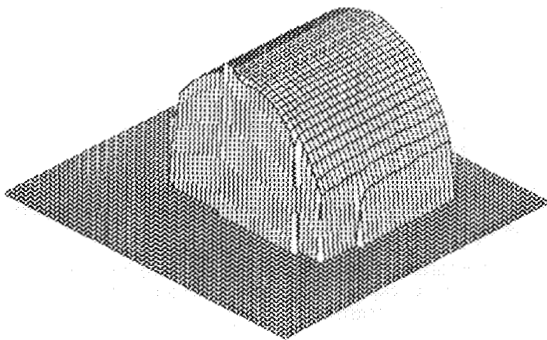
OBJECT

OBJECT

LAMBERTIAN STRENGTH

SPECULAR STRENGTH

LAMBERTIAN STRENGTH
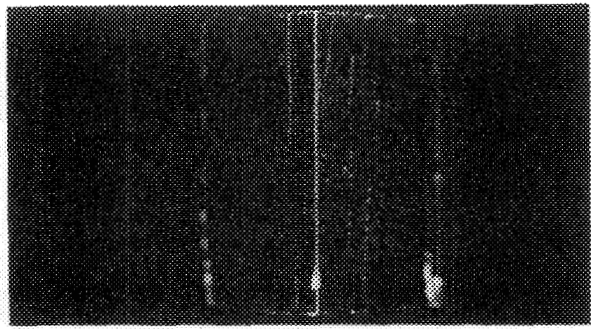
SPECULAR STRENGTH

NEEDLE MAP

NEEDLE MAP

DEPTH MAP
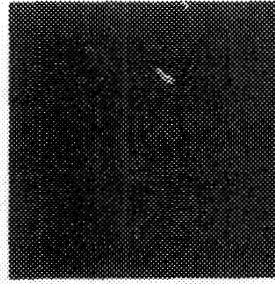
DEPTH MAP

Figure 7: Cylindrical painted object with a Lambertian surface.
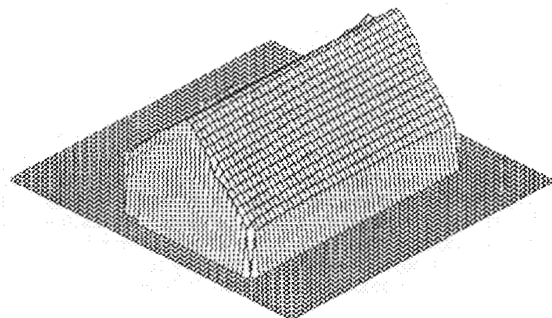
Figure 8: Prism-shaped metallic object with a specular surface.

174

OBJECT
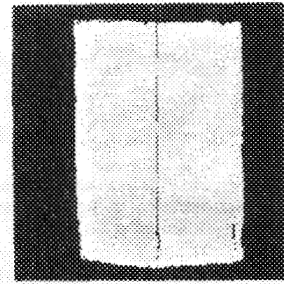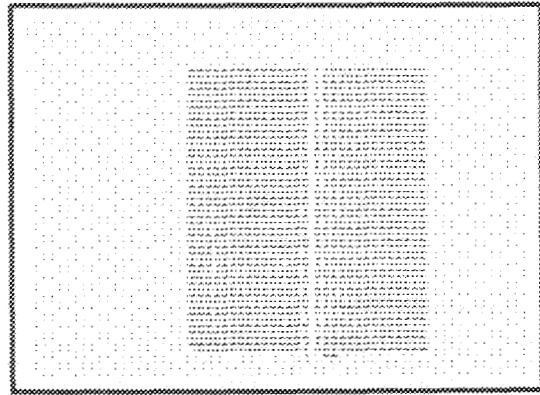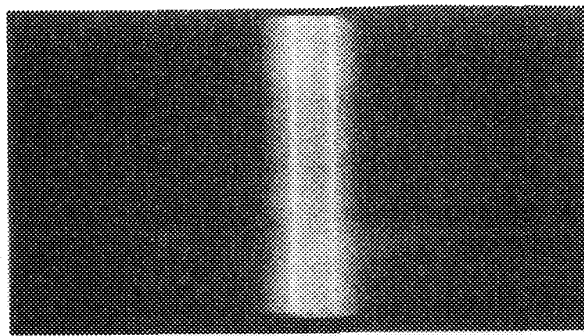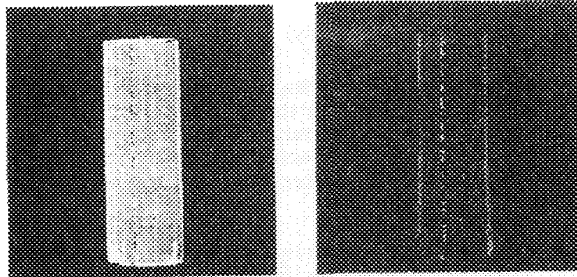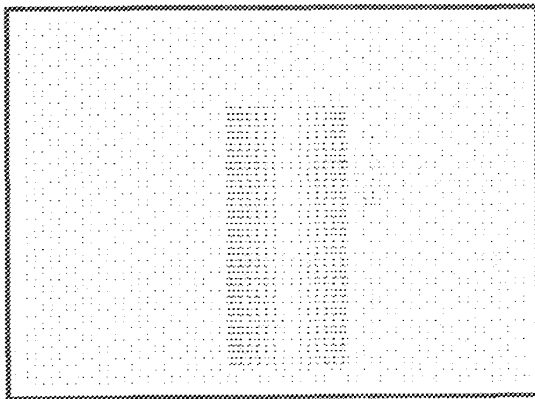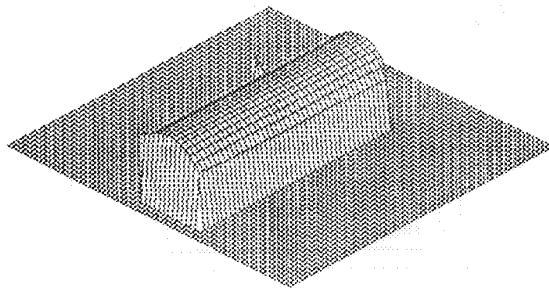

LAMBERTIAN STRENGTH   SPECULAR STRENGTH

NEEDLE MAP

DEPTH MAP

Figure 9: Cylindrical plastic object with a hybrid surface.

References

[1] P. Beckmann and A. Spizzichino, The Scattering of Electromagnetic Waves from Rough Surfaces, The Macmillan Company, 1963.

[2] E. N. Coleman and R. Jain, Obtaining 3-dimensional shape of textured and specular surface using four-source photometry, Computer Graphics and Image Processing, Vol. 18, No. 4, pp. 309-328, April, 1982.

[3] G. Healey and T. O. Binford, Local Shape from Specularity, Proc. Image Understanding Workshop, Vol. 2, pp. 874-887, February, 1987.

[4] B. K. P. Horn, Shape from Shading: A Method for Obtaining the Shape of a Smooth Opaque Object from One View, MIT Project MAC Internal Report TR-79 and MIT AI Laboratory Technical Report 232, November, 1970.

[5] B. K. P. Horn, Image intensity understanding, Artificial Intelligence, Vol. 8, No. 2, 1977.

[6] K. Ikeuchi and B. K. P. Horn, Numerical Shape from Shading and Occluding Boundaries, Artificial Intelligence, Vol. 17, Nos. 1-3, pp. 141-184, August, 1981.

[7] K. Ikeuchi, Determining surface orientations of specular surfaces by using the photometric stereo method, IEEE Trans. on Pattern Analysis and Machine Intelligence, Vol. 3, No. 6, pp. 661-669, November, 1981.

[8] S. K. Nayar, K. Ikeuchi, T. Kanade, Extracting Shape and Reflectance of Lambertian, Specular, and Hybrid Surfaces, CMU-RI-TR-88-14, August, 1988.

[9] A. P. Pentland, Local Shading Analysis, IEEE Trans. on Pattern Analysis and Machine Intelligence, Vol. 6, No. 2, pp. 170-187, March, 1984.

[10] A. C. Sanderson, L. E. Weiss, and S. K. Nayar, Structured Highlight Inspection of specular surfaces, IEEE Trans. on Pattern Analysis and Machine Intelligence, Vol. 10, No. 1, pp. 44-55, January, 1988.

[11] W. M. Silver, Determining Shape and Reflectance Using Multiple Images, S. M. Thesis, Dept. of Electrical Engineering and Computer Science, MIT, Cambridge, Massachusetts, June, 1980.

[12] K. Torrance and E. Sparrow, Theory for Off-Specular Reflection from Roughened Surfaces, Journal of the Optical Society of America, No. 57, pp. 1105-1114, 1967.

[13] R. J. Woodham, Photometric stereo: A reflectance map technique for determining surface orientation from image intensity, Proc. SPIE, Vol. 155, pp. 136-143, 1978.